The Astrophysical Journal, 973:159 (5pp), 2024 October 1 https://doi.org/10.3847/1538-4357/ad6de0

On the Cosmic Variance of the Merger Rate Density of Binary Neutron Stars

Zhiwei Chen[1,2], Youjun Lu[1,2], Jie Wang[1,2], Zhen Jiang[3], Qingbo Chu[1,2], and Xianghao Ma[1,2]
[1] National Astronomical Observatories, Chinese Academy of Sciences, 20A Datun Road, Beijing 100101, People's Republic of China; chenzhiwei171@mails.ucas.ac.cn
[2] School of Astronomy and Space Sciences, University of Chinese Academy of Sciences, 19A Yuquan Road, Beijing 100049, People's Republic of China
[3] Department of Astronomy, Tsinghua University, Beijing 100084, People's Republic of China
Received 2024 July 7; revised 2024 August 7; accepted 2024 August 8; published 2024 September 30

Abstract

The cosmic variance on the star formation history may lead to bias in the merger rate density estimation of binary neutron star (BNS) mergers by compact binary population synthesis. In this paper, we take advantage of the large box size of the Millennium Simulation combined with the semianalytic galaxy formation model GABE and the parameterized population binary star evolution model to examine how much effect the cosmic variance will introduce on the estimation of the merger rate density of BNS mergers. We find that for subbox sizes of 100 and 200 Mpc, the variance of merger rate density σ_R/R at different redshifts is about 23%–35% and 13%–20%, respectively. On the one hand, as for the variance of the detection rate on BNS mergers with the current LIGO–Virgo–KAGRA (LVK) detector network, this value is very small at $\lesssim$10%, which indicates ignoring the cosmic variance is reasonable for estimating the merger rate density from current LVK observations. On the other hand, with next-generation gravitational wave detectors, it is possible to localize BNS mergers within subboxes possessing a length of 40 Mpc for a source redshift $z_s < 0.2$. In such a small box, the cosmic variance of the merger rate density is significant, i.e., the value of σ_R/R is about ∼55%. This hints that estimating the merger rate density of BNS in different sky areas may provide useful information on the cosmic variance.

Unified Astronomy Thesaurus concepts: Gravitational wave astronomy (675); Gravitational wave sources (677)

1. Introduction

The first detection of a gravitational wave (GW) emitted by the binary neutron star (BNS) merger GW170817 and its electromagnetic (EM) counterpart signals marks the beginning of a new era of multimessenger astronomy (e.g., B. P. Abbott et al. 2017a, 2017b, 2019a; D. A. Coulter et al. 2017; E. Pian et al. 2017; D. Dobie et al. 2018; M. W. Coughlin et al. 2019). The associated EM counterpart can provide significant information on the physical properties of BNS mergers, for example, the tidal deformability and the equation of state constrained from the GW, afterglow, and kilonova signals (e.g., O. Gottlieb et al. 2018; X. Xie et al. 2018). Moreover, with the redshift measurement of the EM counterpart and luminosity distance measurement from the GW signal, BNS mergers can be viewed as excellent standard sirens to constrain the cosmological parameters. For example, the Hubble constant can be constrained to a precision of ∼10% by the data of GW170817, GRB170817A, and AT 2017gfo (The LIGO Scientific Collaboration et al. 2021). With the development of ground-based GW detectors, it is anticipated to observe many more GW170817-like objects in the near future, which may constrain H_0 to ∼1% precision.

It is crucial to estimate the evolution of the merger rate density of BNS mergers. The merger rate density of BNS mergers are dependent on the detailed physics embedded in the binary evolution procedure, including the common envelope ejection, Roche lobe mass transfer process, and the production of natal kick (e.g., Q. Chu et al. 2022). For example, if the natal kick is large enough, the BNS may not form at the end of its progenitor life, which may decrease the merger rate density of BNS mergers significantly. Another important recipe is the star formation rate (SFR) evolution of galaxies in our Universe. The lower SFR will result in less compact binary formation and thus lower the merger rate density. Therefore, it is possible to constrain such important physical recipes by comparing the measurement to the results given by compact binary population synthesis.

Cosmological numerical simulation has been widely used to estimate the merger rate density and predict the performance of ground-based GW detectors of double compact objects (e.g., Rauf et al. 2023, 2024). However, almost all the works done so far just simply take an average (global) of the resulted merger rate density in the full box of the hydrodynamical simulations (e.g., M. Dominik et al. 2012, 2013, 2015; S. E. de Mink & K. Belczynski 2015; M. Mapelli & N. Giacobbo 2018; Q. Chu et al. 2022), such as Illustris-TNG (A. Pillepich et al. 2018) and EDGES (J. Schaye et al. 2015), limited by their small box size, normally ∼300 Mpc, while ignoring the potential effect of cosmic variance in our local Universe. This choice may lead to a bias in the merger rate density evolution estimation and therefore the detection rate of BNS mergers, especially in the O2 run of LIGO–Virgo–KAGRA (hereafter LVK) GW detector network (B. P. Abbott et al. 2019b), for its small angle-averaged BNS detection range (∼96 Mpc for the LIGO-Livingston and 80 Mpc for the LIGO-Hanford).

In this paper, we take advantage of the large box size of the Millennium Simulation combined with the semianalytic galaxy formation model GABE and the parameterized population binary stellar evolution (BSE) model of our previous work to examine how much effect the cosmic variance will introduce on the estimation of the merger rate density of BNS mergers. This paper is organized as follows. In Section 2, we briefly introduce the semianalytic galaxy formation model GABE and

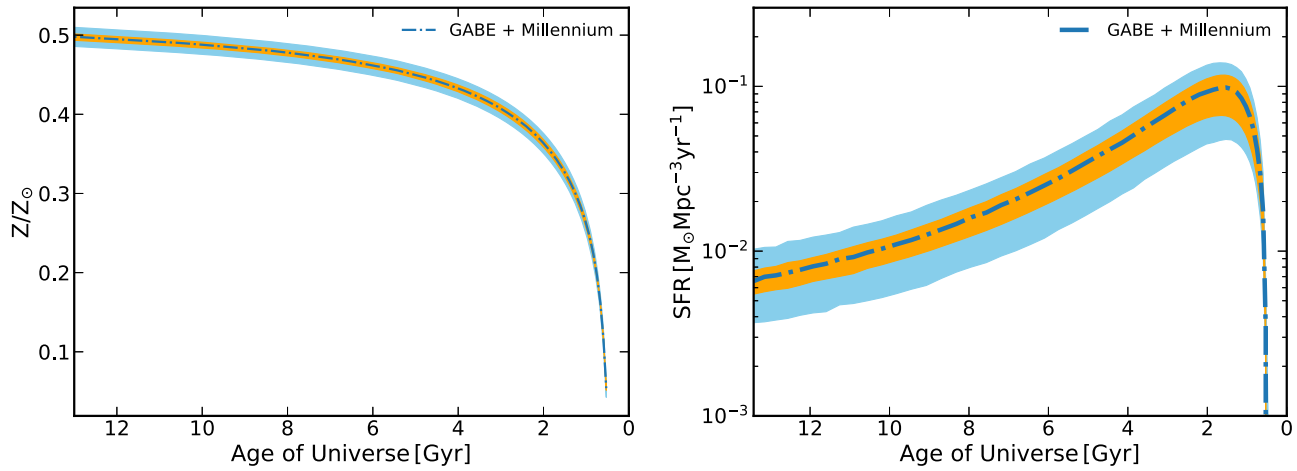

Figure 1. The metallicity evolution (left panel) and SFR density evolution (right panel) with redshift z_s from the GABE semianalytical galaxy formation model together with the Millennium Simulation. The blue dotted–dashed lines show the global results for both metallicity Z and SFR. The inner orange shaded area represents the scatter induced by cosmic variance when $N_{\rm subbox} = 27$ and correspondingly $l_{\rm subbox} = 200$ Mpc, while the outer blue shaded area represents the scatter when $N_{\rm subbox} = 216$ and correspondingly $l_{\rm subbox} = 100$ Mpc.

the key parameters of BSE models. In Section 3, we present the main results. Discussions and conclusions are given in Section 4. Throughout the paper, we adopt the cosmological parameters as $(h_0, \Omega_{\rm m}, \Omega_\Lambda) = (0.68, 0.31, 0.69)$ (N. Aghanim et al. 2020).

2. Simulation Recipes

The semianalytical galaxy formation model GABE and N-body numerical Millennium Simulation (e.g., V. Springel et al. 2005; Z. Jiang et al. 2019) are adopted to estimate the cosmic merger rate density evolution of BNSs. The GABE model considers several important physical processes of galaxy formation, including the cosmic reionization, gas cooling with background radiation, star formation, supernova (SN) feedback, black hole growth, AGN feedback, and bar formation. As for the hierarchical growth of structure formation under the standard cold dark matter model, the tidal and ram pressure stripping of hot gas, dynamical fraction, black hole growth, and star bursts in mergers and bulge formation are taken into account. A more detailed description about galaxy formation and evolution in GABE can be found in Z. Jiang et al. (2019).

The simulation box size is 685 Mpc, and the mass resolution of dark matter is $1.2 \times 10^9 M_\odot$, which allows us to generate a complete galaxy catalog for galaxies more massive than $10^8 M_\odot$. We discrete the full box into 216 and 27 subboxes with box sizes of 100 and 200 Mpc, respectively, which are about the twice the length of the comoving distance of the observed GW170817 ($\sim$50 Mpc) and O2 BNS observation horizon ($\sim$90 Mpc). Note that we do not consider the length scale of the O3-O4a run (R. Abbott et al. 2021, 2023) for their large observation horizon, i.e., $\sim$150–200 Mpc. In such a scale, the cosmic variance is small enough for one to neglect its impact.

The merger rate density evolution of BNSs are mainly dependent on the metallicity and SFR density distribution across the Universe; however, the dependency on metallicity is relatively weak. Therefore, the diversity of the detection rate of BNSs among those subboxes is due to the difference of galaxy formation history in different subboxes caused by cosmic variances. Then, for each subbox, we calculate the evolution of metallicity and SFR for each galaxy through tracing back its formation history by finding out all the progenitors in the whole cosmic merger trees.

Figure 1 shows the metallicity Z (left panel) and SFR evolution (right panel) with redshift z_s obtained from the semianalytical galaxy formation model GABE and Millennium Simulation. The blue dotted–dashed lines show the global (or the median) results for both metallicity Z and SFR evolution, while the inner and outer shaded regions represent the scatter induced by the cosmic variance among 27 subboxes with $l_{\rm subbox} = 200$ Mpc and 216 subboxes with $l_{\rm subbox} = 100$ Mpc, respectively. We note here that for metallicity, our results are slightly higher than those constrained by K. Belczynski et al. (2016) but almost the same as the results in Q. Chu et al. (2022) obtained from EAGLE and Illustris-TNG. Moreover, one can see that the metallicity Z and its evolution are not affected much by the cosmic variance among different subboxes. However, for the SFR density, the cosmic variance can have a significant effect, for which the resulted SFR density may vary by a factor of $\sim$1.3−2. The largest SFR produced in a subbox can be higher than that with the smallest SFR by a factor of more than 3. Though it is currently not clear how much of an effect cosmic variance can introduce to the SFR density within the local volume (P. Madau & M. Dickinson 2014), an observation of a galaxy cluster survey shows that there should be an underdensity in the matter distribution of about $\sim$–30% ± 15% in a region with a radius of about 100 Mpc (H. Böhringer et al. 2020). This may hint that the SFR density in the local volume may be smaller than the average across the universe. Later, we shall see that the the cosmic variance affects the merger rate density of BNS mergers mainly via the scatter of SFR density.

We adopt the parameterized population models proposed in Q. Chu et al. (2022) to mock the binary stellar evolution, including α10.kbβ0.9, α1.kbβ0.9, and γ1.5kbβ0.9. Among these models, the impacts of the common-envelope phase, natal kick, mass ejection during the secondary SN explosion, and metallicity are taken into account. The main differences between these three models are the choice of common-envelope description and the settings of model parameters. Here α and γ denote the conserved energy and conserved angular momentum description in the mass transfer process of the common envelope, respectively. In our previous work,

Table 1
Model Parameters of BSE Models Adopted, i.e., α10.kbβ0.9, α1.kbβ0.9, and γ1.5kbβ0.9

Model	α/γ	σ_k (km s^{-1})	β
α10.kbβ0.9	10	190/30	0.9
α1.kbβ0.9	1.0	190/30	0.9
γ1.5kbβ0.9	1.5	190/30	0.9

Note. Here the first column α/γ represents parameters of the α/γ formalism of the common-envelope ejection process. The second column σ_k is the dispersion of the natal kick distribution, which is assumed to be Maxwellian and bimodal, with $\sigma_k = 190$ km s^{-1} and 30 km s^{-1}, respectively. The third column β represents the ratio of post-SN to pre-SN total system masses, which is set to be 0.9 across these three models. More details about the BSE model can be seen in Q. Chu et al. (2022).

Q. Chu et al. (2022) found that these three models rank the first three in the consistency check with the galactic BNS observations by utilizing the Bayes factor methods. The key model parameters are listed in Table 1, and more details about them can be seen in Q. Chu et al. (2022).

To reduce the cost of computing time, we do not implement the full BSE code into the GABE model together with the Millennium Simulation for each subbox but rather apply the $N_{\rm cor}$ description as discussed in M. Mapelli & N. Giacobbo (2018) to estimate the merger rate density evolution of BNSs $R^i(z_s)$ in the ith discrete subbox as

$$R^i(z_s) = \int dt_{\rm d} P_t(t_{\rm d}) f_{\rm b}\, {\rm SFR}^i(z_{\rm b}) \times N_{\rm cor}(Z^i(z_{\rm b})), \quad (1)$$

where $f_{\rm b}$ denotes the binary formation efficiency (normally $f_{\rm b} = 0.5$), ${\rm SFR}^i(z_{\rm b})$ is the SFR density at the binary formation redshift $z_{\rm b}$ (or time $t_{\rm b}$) in the ith subbox, and $N_{\rm cor}$ is the number of merging BNSs per unit mass in the ith subbox, which is directly related to the star metallicity $Z^i(z_{\rm b})$ at $z_{\rm b}$. The term $t_{\rm d}(z_{\rm b}) = \int_{z_s}^{z_{\rm b}} |\frac{dt}{dz}| dz$ denotes the time delay of a BNS merger from its progenitor binary star formation time, and $P_t(t_{\rm d})$ is its probability distribution, ranging from 10 Myr to a Hubble time $t_{\rm H}$. Here we argue that the above estimation based on this simplified description is solid for $N_{\rm cor}$ and is only related to the metallicity Z and different BSE models. Figure 2 shows the dependence of $N_{\rm cor}$ as function of the binary progenitor's metallicity Z simulated by Q. Chu et al. (2022). As seen from this figure, the value of $N_{\rm cor}$ can vary by a factor of 1−2, considering different metallicities in different BSE models. This is due to the small mass range of NSs, regardless of whether it is formed through iron core-collapse or electron-capture SNe.

3. Results

We obtain the the merger rate density evolution R^i of the BNS mergers in each subbox as well as the global one from the whole box of the Millennium Simulation by integrating Equation (1) over all the snapshots of our cosmological simulation, i.e., $z_s \sim 0$–10 for 64 snapshots. Figure 3 shows the results of the merger rate density and its evolution by adopting the BSE model α10.kbβ0.9. As seen from this figure, despite the slight bias of the median value ($R(z_s = 0) \sim 279$ Gpc^{-3} yr^{-1} in our simulation), there is variation on $R(z_s)$ across the

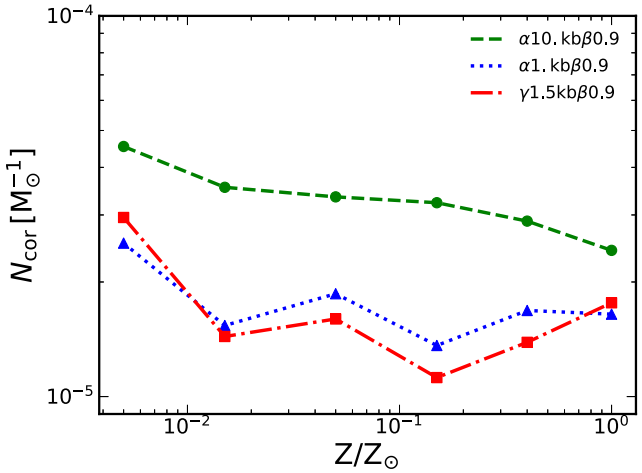

Figure 2. The relationship between the number of merging BNSs per unit mass ($N_{\rm cor}$) and the binary progenitor's metallicity (Z) simulated in Q. Chu et al. (2022). The green dashed, blue dotted, and red dotted–dashed lines show the results of different parameterized population models, i.e., α10.kbβ0.9, α1. kbβ0.9, and γ1.5kbβ0.9, respectively.

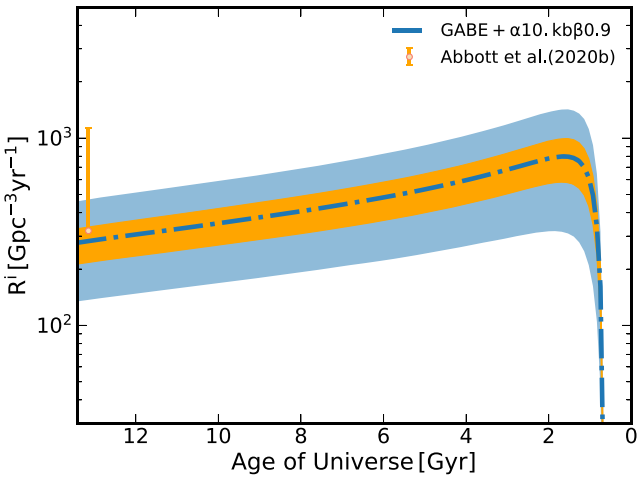

Figure 3. The comoving merger rate density evolution of BNS mergers R^i as a function of the age of universe obtained by adopting the α10.kbβ0.9 BSE model. The blue dotted–dashed line shows the global results obtained by using the whole simulation box of the Millennium Simulation, and the inner orange and outer blue shaded regions show the scatter of R^i induced by the cosmic variance among the 27 and 216 discrete subboxes with sizes of $l_{\rm subbox} = 100$ and 200 Mpc, respectively. The orange dot with an error bar marks the local merger rate density obtained from the GW detections of the two BNS mergers (GW170817 and GW190425; R. Abbott et al. 2020), i.e., $R(z_s = 0) \sim 320^{+490}_{-240}$ Gpc^{-3} yr^{-1}.

subboxes due to the cosmic variance. For example at the same redshift, the largest R is almost twice the value of the smallest R assuming $l_{\rm subbox} = 100$ Mpc, for the SFR density in this subbox is much higher.

To quantify the effect of cosmic variance on the merger rate density and the detection rate, we define the relative variance of a random variable X with cumulative probability distribution $P(X)$ by the following expression:

$$\frac{\sigma_X}{X} = \frac{X(P(X) = 0.84) - X(P(X) = 0.16)}{2X(P(X) = 0.5)}. \quad (2)$$

Figure 4 further plots the evolution of the relative variance σ_R/R with redshift z_s for these three models, assuming the subbox sizes to be 100 (top panel) and 200 Mpc (bottom panel). As seen from

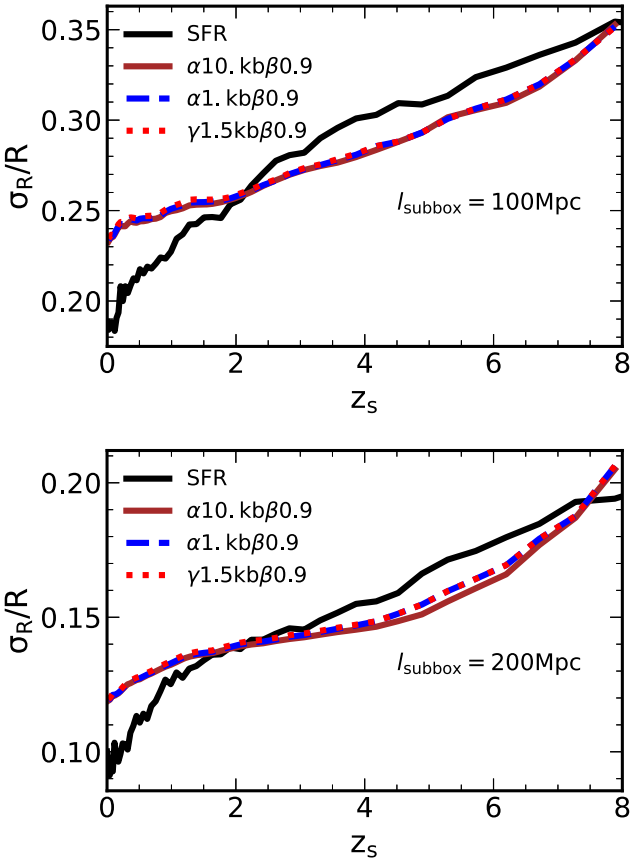

Figure 4. The evolution of the relative variance $\sigma(R)/R$ with redshift z_s with different subbox lengths, i.e., $l_{\rm subbox} = 100$ (upper panel) and $l_{\rm subbox} = 200$ Mpc (bottom panel). The brown solid, blue dashed, and red dotted lines show the results of different parameterized population models, i.e., α10.kbβ0.9, α1.kbβ0.9, and γ1.5kbβ0.9 respectively. The black solid line shows the relative variance on the SFR.

this figure, the smaller the subbox size, the higher the relative variance at a given redshift. For example, the local relative variance σ_R/R is about ∼23.5% and ∼12.0% for $l_{\rm subbox} \sim 100$ (top panel) and 200 Mpc, respectively. This is easy to understand, for the inhomogeneity of star formation decreases with the box size of the simulation, assuming a Gaussian random field. In addition, the evolution and scatter σ_R/R resulting from different models are quite similar, though the exact values of $R^i_{z_s}$ are different. This fact indicates that the estimation on σ_R/R can be viewed as reasonable and reliable, and their dependence on the choices of different binary population synthesis parameters is weak.

Moreover, the value of σ_R/R increases with increasing redshift, which can be mainly explained by the star formation history: the inhomogeneity of star formation is much higher, for voids more commonly exist at early times. As seen from Figure 4, compared with the variance of the SFR, σ_R/R is suppressed before $z_s \sim 2$ for different subbox size cases. This is mainly due to the time delay from the binary star formation to their merger, which may flatten the difference of different boxes due to the integration effect.

With next-generation ground-based GW detectors, it is possible to localize BNS mergers within a very small area. For example, with Cosmic Explorer (CE) networks, BNS mergers below $z_s \sim 0.2$ are expected to be localized within the sky area

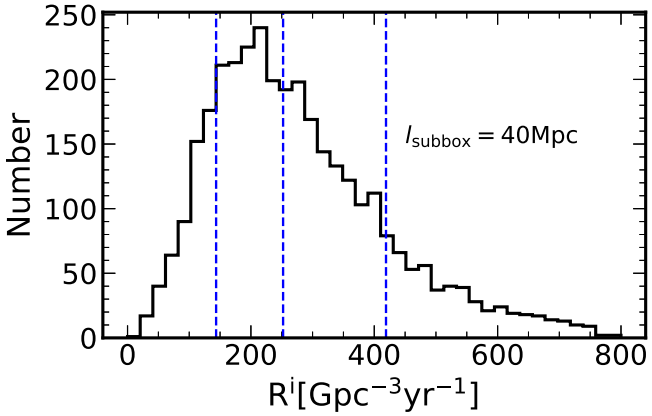

Figure 5. The distribution of the BNS merger rate density of $15 \times 15 \times 15$ realization of subboxes, assuming a α10.kbβ0.9 BSE model. The length of the subbox is set to be 40 Mpc, which corresponds to the localization precision of CE networks. The blue dashed lines from left to right show the 16%, 50%, and 84% quantiles of the distribution.

of $\Delta\Omega_s \sim 0.10\,{\rm deg}^2$ and $\Delta d_L \sim 20$ Mpc (W. Zhao & L. Wen 2018). In such a small comoving volume, the impact of cosmic variance can be very large. We calculate the distribution of merger rate density with a subbox size of 40 Mpc at $z_s = 0.2$, and the resulting distribution is shown in Figure 5. It can be seen that the relative variance σ_R/R is much larger, i.e., ∼55%. This result indicates that with future next-generation ground-based GW detectors, estimating the merger rate density of BNS in different sky areas may also provide useful information on the cosmic variance.

With the merger rate density evolution estimated by our ranked-first model α10.kbβ0.9, we may further check the variance on the detection rate of BNS mergers in the O2 run, σ_N/N, induced by the cosmic variance, following the standard Monte Carlo procedure. We refer the readers to Y. Zhao & Y. Lu (2021) and Z. Chen (2023) for details on the generation of mock BNS samples and their SNR calculation. We find that the variance on detection rate is ∼13% for the detection threshold $\varrho_0 = 12$ and ∼9% for $\varrho_0 = 8$. For GW observation runs post-O2, the variance is much smaller at $\lesssim$5%. During the writing procedure of this paper, we noted that G. Morras & J. Garcia-Bellido (2024) also consider the effects of local cosmic inhomogeneities on the GW event rate but simply assume the merger rate is proportional to the matter density. Using the peculiar velocities of galaxies from the CosmicFlows catalogs, they find the cosmic variance effect on the compact binary coalescence event rate to be at most ∼6%, which is almost consistent with our results. Therefore, we conclude that the estimation of the local merger rate density from the current observation of LVK is safe by ignoring the cosmic variance because of their very small impact on the detection rate. Here we also noticed that based on the observation of the galaxy cluster survey, the density of local volume (within 100 Mpc radius) is ∼30% underdense from the average across the Universe, which indicates that the detection rate of BNS mergers per comoving volume in our local Universe may be smaller than the average value across the universe by a factor of ∼1%–5%.

4. Discussions and Conclusions

In this work, we test the effect of cosmic variance on the merger rate density of BNS by adopting the galaxy formation

model GABE based on the *n*-body numerical Millennium Simulation and the BNS population synthesis model.

We find that for subbox sizes of 100 Mpc and 200 Mpc, the relative variance of the merger rate density σ_R/R at different redshifts is about 0.23−0.35 and 0.13−0.20, respectively. With future powerful next-generation GW detectors, it is anticipated to detect $\sim 10^3$–10^4 BNS mergers. This indicates that one may constrain the cosmic variance via the estimation of the BNS merger rate density in different sky areas. Moreover, we estimate the variance on the detection rate of BNS mergers induced by the cosmic variance. We find that the relative variance of the detection rate is about $\sigma(N)/N \sim 0.05-0.1$, which is small enough to not significantly impact the inferred merger rate density. As for future next-generation GW detectors, it is possible for one to localize BNS mergers into small subboxes. In such a small comoving volume, the impact of cosmic variance on the merger rate density and therefore the detection number is much more significant. This offers a possible approach to constrain the cosmic variance by the spatial analysis of BNS mergers.

Note here that as the first estimation, there are many complexities we may need to further take into account. For example, the absolute value of both σ_R/R and σ_N/N may vary slightly due to different settings in the semianalytical simulations. Moreover, to reduce the cost of computing, we did not run full population synthesis in each subbox but used simple descriptions of BNS mergers by the SFR and metallicity to estimate the σ_R/R. This may also lead to slight differences in the results, though this does not affect our main claim.

One may also conduct a parallel analysis on the stellar binary black hole mergers to check the effect of cosmic variance on their merger rate density. Besides, it is also possible to find a small subbox very similar to our local observation in this model, which may provide interesting insights into the estimation of the local merger rate density of compact binaries. We defer these aspects to future work.

Acknowledgments

Z.C. thanks the daily AstroCoffee organized in the National Astronomical Observatories of China and the speakers and audiences therein for their helpful discussions. This work is partly supported by the Strategic Priority Research Program of the Chinese Academy of Sciences (grant No. XDB0550300), the National Natural Science Foundation of China (grant Nos. 12273050 and 11991052), and the National Key Program for Science and Technology Research and Development (grant Nos. 2020YFC2201400 and 2022YFC2205201).

ORCID iDs

Zhiwei Chen https://orcid.org/0000-0001-7952-7945
Youjun Lu https://orcid.org/0000-0002-1310-4664
Jie Wang https://orcid.org/0000-0002-9937-2351

References

Abbott, B. P., Abbott, R., Abbott, T. D., et al. 2017a, ApJL, 848, L12
Abbott, B. P., Abbott, R., Abbott, T. D., et al. 2017b, ApJL, 848, L13
Abbott, B. P., Abbott, R., Abbott, T. D., et al. 2019a, PhRvX, 9, 011001
Abbott, B. P., Abbott, R., Abbott, T. D., et al. 2019b, PhRvX, 9, 031040
Abbott, R., Abbott, T. D., Abraham, S., et al. 2020, ApJL, 896, L44
Abbott, R., Abbott, T. D., Abraham, S., et al. 2021, PhRvX, 11, 021053
Abbott, R., Abbott, T. D., Acernese, F., et al. 2023, PhRvX, 13, 041039
Aghanim, N., Akrami, Y., Ashdown, M., et al. 2020, A&A, 641, A6
Belczynski, K., Holz, D. E., Bulik, T., & O'Shaughnessy, R. 2016, Natur, 534, 512
Böhringer, H., Chon, G., & Collins, C. A. 2020, A&A, 633, A19
Chen, Z. 2023, ApJ, 953, 36
Chu, Q., Yu, S., & Lu, Y. 2022, MNRAS, 509, 1557
Coughlin, M. W., Dietrich, T., Margalit, B., & Metzger, B. D. 2019, MNRAS, 489, L91
Coulter, D. A., Foley, R. J., Kilpatrick, C. D., et al. 2017, Sci, 358, 1556
de Mink, S. E., & Belczynski, K. 2015, ApJ, 814, 58
Dobie, D., Kaplan, D. L., Murphy, T., et al. 2018, ApJL, 858, L15
Dominik, M., Belczynski, K., Fryer, C., et al. 2012, ApJ, 759, 52
Dominik, M., Belczynski, K., Fryer, C., et al. 2013, ApJ, 779, 72
Dominik, M., Berti, E., O'Shaughnessy, R., et al. 2015, ApJ, 806, 263
Gottlieb, O., Nakar, E., Piran, T., & Hotokezaka, K. 2018, MNRAS, 479, 588
Jiang, Z., Wang, J., Gao, L., et al. 2019, RAA, 19, 151
Madau, P., & Dickinson, M. 2014, ARA&A, 52, 415
Mapelli, M., & Giacobbo, N. 2018, MNRAS, 479, 4391
Morras, G., & Garcia-Bellido, J. 2024, arXiv:2406.00691
Pian, E., D'Avanzo, P., Benetti, S., et al. 2017, Natur, 551, 67
Pillepich, A., Nelson, D., Hernquist, L., et al. 2018, MNRAS, 475, 648
Rauf, L., Howlett, C., Davis, T. M., & Lagos, C. D. P. 2023, MNRAS, 523, 5719
Rauf, L., Howlett, C., Stevenson, S., & Riley, J. 2024, arXiv:2406.11885
Schaye, J., Crain, R. A., Bower, R. G., et al. 2015, MNRAS, 446, 521
Springel, V., White, S. D. M., Jenkins, A., et al. 2005, Natur, 435, 629
The LIGO Scientific Collaboration, the Virgo Collaboration, the KAGRA Collaboration, et al. 2021, arXiv:2111.03634
Xie, X., Zrake, J., & MacFadyen, A. 2018, ApJ, 863, 58
Zhao, W., & Wen, L. 2018, PhRvD, 97, 064031
Zhao, Y., & Lu, Y. 2021, MNRAS, 500, 1421